2003

Analysis of Molten Carbonate Fuel Cell Performance Using a Three-Phase Homogeneous Model

N. Subramanian
University of South Carolina - Columbia

B. S. Haran
University of South Carolina - Columbia

P. Ganesan
University of South Carolina - Columbia

Ralph E. White
University of South Carolina - Columbia, white@cec.sc.edu

Branko N. Popov
University of South Carolina - Columbia, popov@engr.sc.edu

Publication Info

Journal of the Electrochemical Society, 2003, pages A46-A56.

Publisher's link: http://dx.doi.org/10.1149/1.1522721
DOI: 10.1149/1.1522721

Journal of The Electrochemical Society, **150** (1) A46-A56 (2003)
0013-4651/2002/150(1)/A46/11/$7.00 © The Electrochemical Society, Inc.

Analysis of Molten Carbonate Fuel Cell Performance Using a Three-Phase Homogeneous Model

N. Subramanian,* B. S. Haran, P. Ganesan,* R. E. White,*** and B. N. Popov**,z**

Department of Chemical Engineering, University of South Carolina, Columbia, South Carolina 29208, USA

In this study a three-phase homogeneous model was developed to simulate the performance of the molten carbonate fuel cell (MCFC) cathode. The homogeneous model is based on volume averaging of different variables in the three phases over a small volume element. This approach can be used to model porous electrodes as it represents the real system much better than the conventional agglomerate model. Using the homogeneous model the polarization characteristics of the MCFC cathode was studied under different operating conditions.
 [DOI: 10.1149/1.1522721]

Manuscript submitted April 23, 2002; revised manuscript received June 18, 2002. Available electronically November 15, 2002.

Molten carbonate fuel cells (MCFCs) are currently in development for stationary power sources. With high efficiencies and low pollution problems, these high temperature fuel cells are ideally suited for reducing our reliance on gasoline. The state of the art MCFC cathode is porous NiO. However, under the corrosive conditions prevalent at high temperatures, nickel oxide dissolves in the melt. This slow loss of active material contributes to an increase in the overall cell resistance thereby reducing the energy density and power density of the fuel cell stack. Alternate cathodes such as $LiCoO_2$ and $LiFeO_2$ have been tried to avoid the dissolution problems faced with NiO. However, these materials suffer from lower reaction kinetics and/or higher ohmic resistance as compared to nickel oxide. The search for alternate cathode materials could be simplified through the use of theoretical models, which simulate the performance of the MCFC cathode under a wide range of operating conditions. It is also desirable to study the influence of various electrode design parameters on the polarization behavior of the MCFC cathode.

Several theoretical models have been derived for the molten carbonate fuel cathode[1-11] First principles based theoretical models for MCFC cathode can be divided into the thin film model[1] and the agglomerate model.[2] Wilemski[1] assumed that the MCFC cathode could be described as a cylindrical pore covered with a thin film of electrolyte. Gases flowing through the pore dissolve at the surface of the film and diffuse to the surface of the pore and react there. While the model gives good agreement with experimental data, it requires knowledge of the pore diameter, length, and film thickness. Further, the entire description of the electrode is limited and cannot be used for cathode design analysis or two-dimensional simulations. The more common and popular approach for describing the MCFC cathode is the agglomerate model proposed by Yuh and Selman.[2] In this approach, the electrode is assumed to consist of cylindrical agglomerates completely flooded with electrolyte. Gaseous species move through straight cylindrical channels of macropores. Figure 1 presents a schematic of the agglomerate model as applied to the MCFC cathode. As shown in the figure, the macropore is continuous and extends from the current collector to the aluminate matrix. Adjacent to these macropores are microporous agglomerates covered with a film of electrolyte. Both the macropores and micropores remain segregated and the electrochemical reaction proceeds both on the film (exterior to the agglomerate) and also in the micropores (interior of the agglomerate). Yu and Selman[2] do not consider the varying degree of electrolyte fill in the cathode. Using this model, the polarization characteristics of both the cathode and anode have been analyzed. Further, this approach has also been applied to determine the reaction kinetic parameters through impedance analysis. The performance of the MCFC cathode has been analyzed extensively using the agglomerate model by Prins-Jansen *et al.*[3] Kunz *et al.*[4] used the agglomerate approach but assumed that the reaction proceeded only on the interior surface of the agglomerate but not on the surface of the film. Further, they incorporated the varying electrolyte fill in the cathode by correlating the porosimetry data to the agglomerate diameter. Fontes *et al.*[5] modified Selman's agglomerate model[2] to account for the electrolyte fill and compared these results to those of Kunz *et al.*[4] They accounted for the increase in the amount of electrolyte by the uniform growth of the electrolyte film or the decrease of the effective surface area for the reaction. They found that a partially drowned agglomerate model with consideration of reaction on the exterior agglomerate surface provided a more realistic description of the cathode as compared to the homogeneous agglomerate model. Christensen and Livbjerg[6] who considered the agglomerate as a one-dimensional slab instead of a cylinder also used a similar approach.

The principal deficiency of the agglomerate model, apart from the simplified pore structure assumed, is the lack of measured values for film thickness and agglomerate radius. Both these parameters cannot be estimated appropriately. The agglomerate radius can be estimated from post-test scanning electron microscopy (SEM) micrographs. However, this radius is not the same along the whole length of the electrode. Further, as discussed by Prins-Jansen *et al.*[3] attempts to estimate the thickness of the film vary by two orders of magnitude. Also, using the agglomerate model it is not possible to determine potential/current variations in directions perpendicular to the depth of the electrode. A pseudo-2D model was used by Fontes *et al.*[7] to determine the effect of different design parameters on the performance of the MCFC cathode. In this approach the local reaction rate was solved separately using the agglomerate approach. This was input as a source function in solving for the potential/current variations in two dimensions. This approach does not convey the true physical picture and is still limited due to the decoupling of the potential from the reaction rate and the use of the agglomerate radius.

The above problems associated with the agglomerate model can be avoided if we take the alternate approach, namely the volume-averaging technique used for porous media as done by Prins-Jansen *et al.*[8] and De Vidts.[12,13] As compared to the agglomerate model where macropores and micropores remain as separate entities, in this approach the pores in the electrode exist in a single continuum. Further, all three phases coexist within the porous electrode and reaction proceeds everywhere at the solid/melt interface. Using the volume-averaging technique, Prins-Jansen *et al.*[8] developed an impedance model for extracting the reaction and transport parameters from experimental data. Model simulations were fitted to experimental data within a certain confidence interval. They found that the diffusion coefficient of O_2 and CO_2 is three orders of magnitude

* Electrochemical Society Student Member.
** Electrochemical Society Active Member.
*** Electrochemical Society Fellow.
z E-mail: popov@engr.sc.edu

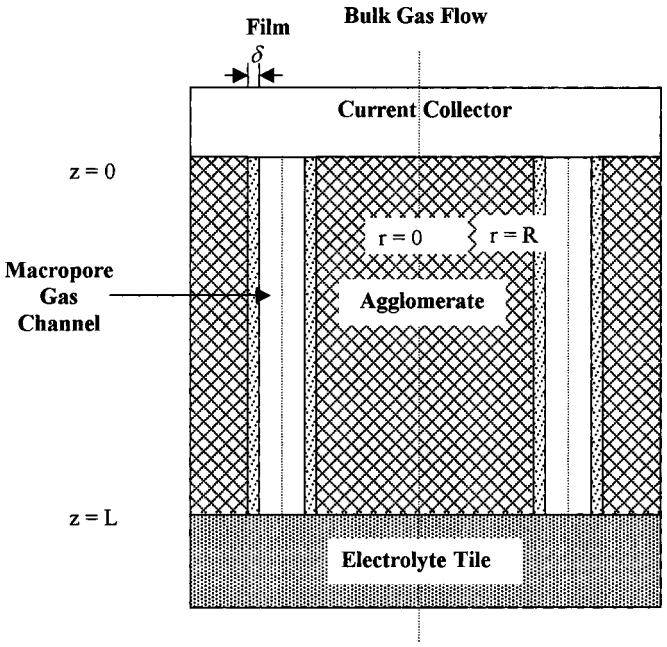

Figure 1. Schematic of the MCFC cell.

larger than that estimated from the agglomerate model. Other parameters were of the same magnitude as reported by Yuh and Selman.[2]

The model developed by Prins-Jansen *et al.*[8] combines both the electrolyte and gas phases into a single entity during volume averaging. The gas- and liquid-phase mass transport were not considered separately. In this paper, we adopt the volume-averaging technique as outlined by De Vidts and White[12] for three-phase reactions in porous electrodes. Using this approach, volume-averaged concentrations of both gaseous- and liquid-phase reactants are obtained separately. The goal of this study was to use the volume-averaging technique for studying the polarization characteristics of the MCFC cathode, which has not been done before. The effect of different design parameters on the electrode performance has also been analyzed. The model considers the potential and current variation in both liquid and solid phases. Further concentration variations in the liquid and gaseous phases are considered separately. Using this approach electrolyte filling can be incorporated easily in addition to eliminating the problems associated with the agglomerate concept. Also different reaction mechanisms can be studied and homogeneity can be assumed safely.

Development of a Theoretical Model

In the molten carbonate fuel cell, oxygen and CO_2 combine at the cathode to form carbonate ions. At the anode hydrogen combines with the carbonate ions from the cathode to form CO_2 and water. The net reaction results in the formation of water with no harmful side reactions. The system of interest to us is the cathode where reduction of oxygen occurs. In order to overcome the difficulties associated with the agglomerate approach, we start by considering a cross section of the porous electrode as shown in Fig. 2. No difference is made between the macropores and micropores while deriving the model equations. The primary reaction in the MCFC cathode is oxygen reduction, which is given by

$$\frac{1}{2}O_2 + CO_2 + 2e^- \rightarrow CO_3^{2-} \qquad [1]$$

The above reaction occurs at the interface between the NiO particle and the electrolyte. We neglect any changes in the concentration of the carbonate ions and assume that the concentration of the electrolyte does not change. Further, we assume that the system is at steady state and neglect any changes in the cathode due to corrosion. Finally, we neglect changes in temperature in the cathode. Based on these assumptions we next derive the volume-averaged equations describing transport and reaction in the MCFC cathode.

Concepts and definitions of volume averaging.—In this section, equations are derived for a porous electrode consisting of three phases, solid, liquid, and gas. Following De Vidts and White[12] and De Vidts,[13] we consider a small elemental volume V. This volume should be small compared to the overall dimensions of the porous electrode. But it should be large enough to contain all three phases (see Fig. 2). Also it should result in meaningful local average properties. This volume is so chosen that adding pores around this volume does not result in a change in the local average properties. We avoid the bimodal pore distribution where we consider macropores to be filled with the gas and micropores to be occupied by the electrolyte. Rather pores of all sizes are filled with both the electrolyte and the gas, which is more realistic. Some basic definitions of volume averaging have to be presented before understanding the development of the model equations.

Superficial volume average $\overline{\psi}$ and the intrinsic volume average $\langle\psi\rangle$ are defined as

$$\overline{\psi}^{(i)} \equiv \frac{1}{V}\int_{V_{(i)}} \psi dV \qquad [2]$$

$$\langle\psi\rangle^{(i)} \equiv \frac{1}{V_{(i)}}\int_{V_{(i)}} \psi dV \qquad [3]$$

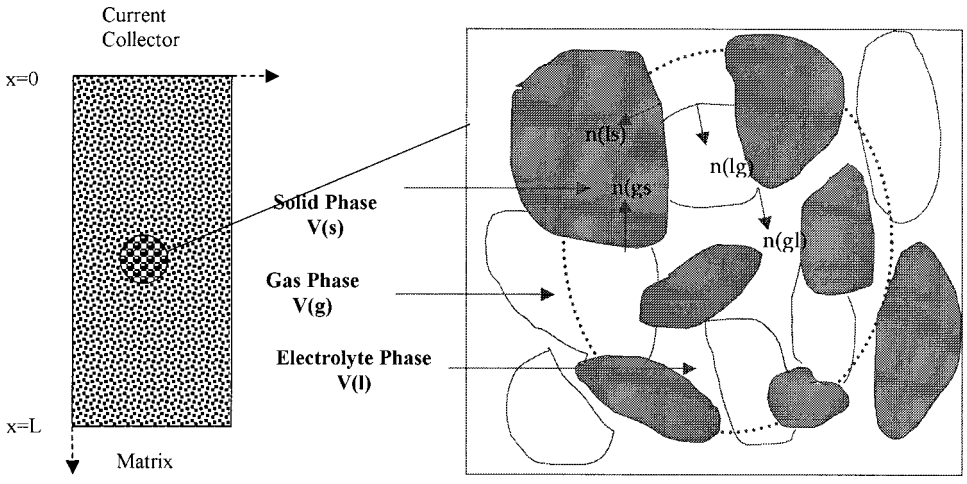

Figure 2. Volume averaging in porous electrode.

Here the superscript i represents the phase. The superficial and intrinsic volume averages are related by the porosity

$$\overline{\psi}^{(i)} = \varepsilon^{(i)}\langle\psi\rangle^{(i)} \quad [4]$$

Whenever volume averages of the gradients and the divergence appear, they should be replaced by the gradients and divergence of the volume averages as below. These are referred to as the theorem of the local volume average of the gradient and the divergence[14,15]

$$\overline{\nabla\psi}^{(l)} = \nabla\overline{\psi}^{(l)} + \frac{1}{V}\int_{S_{lg}}\psi^{(l)}n_{(lg)}dS + \frac{1}{V}\int_{S_{ls}}\psi^{(l)}n_{(ls)}dS \quad [5]$$

$$\overline{\nabla\cdot\psi}^{(l)} = \nabla\cdot\overline{\psi}^{(l)} + \frac{1}{V}\int_{S_{lg}}\psi^{(l)}\cdot n_{(lg)}dS + \frac{1}{V}\int_{S_{ls}}\psi^{(l)}\cdot n_{(ls)}dS \quad [6]$$

Mass transport equations.—Mass transport occurs in the liquid and gas phases. Both oxygen and carbon dioxide gas are fed to the MCFC cathode through the current collector. Both O_2 and CO_2 diffuse through the macropores in the cathode and are transferred by diffusion in the melt to the surface of the NiO particles. The material balance in the liquid and gas phases for any species i is given by

$$\frac{\partial c_i^{(l)}}{\partial t} + \nabla\cdot N_i^{(l)} = 0 \quad i = CO_2,\ O_2 \quad [7]$$

$$\frac{\partial c_i^{(g)}}{\partial t} + \nabla\cdot N_i^{(g)} = 0 \quad [8]$$

There are no bulk reactions. All reactions are assumed to take place at the electrolyte-electrode interface. This is denoted by the normal vector $\mathbf{n}_{(ls)}$ in Fig. 2. Gas diffuses into the electrolyte at the normal interface $\mathbf{n}_{(gl)}$ and reacts at the interface of the electrolyte with the solid catalyst particles, $\mathbf{n}_{(ls)}$. Hence the homogeneous reaction rate is neglected. Fick's law gives molar flux in the liquid and gas phases

$$N_i^{(l)} = -D_i^{(l)}\nabla c_i^{(l)} + c_i^{(l)}v^{\diamond} \quad [9]$$

Binary diffusion is assumed in the gas phase. For a binary system $j_{(A)}$, defined as the mass flux relative to the mass average velocity, is given by[13]

$$j_{(A)} = -\frac{c^2}{\rho}M_{(A)}M_{(B)}D_{(AB)}\nabla x_{(A)} \quad [10]$$

where A refers to O_2 and B refers to CO_2.

The relation between $J_{(A)}^{\diamond}$ (molar flux relative to molar average velocity), $j_{(A)}^{\diamond}$ (mass flux relative to molar average velocity), and $j_{(A)}$ for a binary system is given by

$$J_{(A)}^{\diamond} = \frac{j_{(A)}^{\diamond}}{M_{(A)}} \quad [11]$$

$$j_{(A)}^{\diamond} = \frac{M}{M_{(B)}}j_{(A)} \quad [12]$$

The relation between $N_{(A)}$ (molar flux with respect to a fixed frame of reference) and $J_{(A)}^{\diamond}$

$$J_{(A)}^{\diamond} = N_{(A)} - c_{(A)}v^{\diamond} \quad [13]$$

When convection is neglected

$$N_{(A)} = J_{(A)}^{\diamond} \quad [14]$$

Hence

$$N_{(A)} = -cD_{(AB)}\nabla x_{(A)} \quad [15]$$

$$x_{(A)} = \frac{c_{(A)}}{c} \quad [16]$$

$$N_{(A)} = \frac{c_{(A)}}{c}D_{(AB)}\nabla c - D_{(AB)}\nabla c_{(A)} \quad [17]$$

In general for a binary gas the flux is given by

$$N_i^{(g)} = -D_i^{(g)}\nabla c_i^{(g)} + D_i^{(g)}\left(\frac{c_i^{(g)}}{c^{(g)}}\right)\nabla c^{g} \quad [18]$$

Using the definitions of volume averaging we obtain the volume averaged flux in both phases as

$$\overline{N}_i^{(l)} = -D_i^{(l)}(\varepsilon^{(l)})^{b-1}\nabla(\varepsilon^{(l)}\langle c_i\rangle^{(l)}) \quad [19]$$

$$\overline{N}_i^{(g)} = -D_i^{(g)}(\varepsilon^{(g)})^{b-1}\nabla(\varepsilon^{(g)}\langle c_i\rangle^{(g)}) + D_i^{(g)}(\varepsilon^{(g)})^{b-1}\frac{\langle c_i\rangle^{(g)}}{\langle c\rangle^{(g)}}\nabla(\varepsilon^{(g)}\langle c\rangle^{(g)}) \quad [20]$$

Volume averaging Eq. 7 and 8 and substituting the above definitions in Eq. 19 and 20 gives the following volume-averaged mass balance equations

$$\frac{\partial\overline{c}_i^{(l)}}{\partial t} + \nabla\cdot\overline{N}_i^{(l)} + \overline{F}_i^{(lg)} - \overline{R}_i^{ls} = 0 \quad [21]$$

$$\frac{\partial\overline{c}_i^{(g)}}{\partial t} + \nabla\cdot\overline{N}_i^{(g)} - \overline{F}_i^{(lg)} - \overline{R}_i^{gs} = 0 \quad [22]$$

where $\overline{F}_i^{(lg)}$, $\overline{R}_i^{ls}$, and $\overline{R}_i^{gs}$ are all terms derived from jump balance analysis which has been discussed in detail by De Vidts and White.[12] $\overline{F}_i^{(lg)}$ is the flux of species i from the liquid to the gas phase, $\overline{R}_i^{ls}$ the rate of heterogeneous reaction at the liquid solid interface, and $\overline{R}_i^{gs}$ at the gas solid interface

$$\overline{F}_i^{(lg)} = a^{(lg)}r_i^{(lg)} \quad [23]$$

$$r_i^{(lg)} = k_i^{(lg)}\left(\frac{\langle c_i\rangle^{(l)}}{K_{e,i}} - \langle c_i\rangle^{(g)}\right) \quad [24]$$

where for any species i, k_i is the mass-transfer coefficient and $K_{e,i}$ is the distribution coefficient. Rate of production of species i at the solid liquid interface is expressed in terms of the local current density. Butler-Volmer kinetics is assumed for the reaction at the electrode electrolyte interface

$$\overline{R}_i^{(ls)} = -\sum_k \frac{s_{ik}a^{(sl)}}{n_kF}\langle j_k\rangle^{(sl)} \quad [25]$$

$$\langle j_k\rangle^{(sl)} = i_0\left\{\left(\frac{\langle c_{CO_2}\rangle^{(l)}}{\langle c^*_{CO_2}\rangle^{(l)}}\right)^{p_1}\left(\frac{\langle c_{O_2}\rangle^{(l)}}{\langle c^*_{O_2}\rangle^{(l)}}\right)^{p_2}\exp\left(\frac{\alpha_aF\phi}{RT}\right) - \left(\frac{\langle c_{CO_2}\rangle^{(l)}}{\langle c^*_{CO_2}\rangle^{(l)}}\right)^{q_1}\left(\frac{\langle c_{O_2}\rangle^{(l)}}{\langle c^*_{O_2}\rangle^{(l)}}\right)^{q_2}\exp\left(\frac{-\alpha_cF\phi}{RT}\right)\right\} \quad [26]$$

Here $\langle j_k\rangle^{(sl)}$[16] is the local current density at the solid-liquid interface and i_0 and i_0^0 are the concentration dependent and concentration independent exchange current densities, respectively.[16] The anodic and cathodic reaction orders p_1, p_2, and q_1, q_2 have values of -2, 0, -1, and 1/2, respectively

$$i_0 = i_0^0(p^*_{CO_2})^{r_1}(p^*_{O_2})^{r_2} \quad [27]$$

where r_1 and r_2 have a value of -1.25 and 0.375, respectively, for the peroxide mechanism. These values will be different for other mechanisms.[3] At the gas-solid interface there is no reaction. Hence

$$\overline{R_i^{(gs)}} = 0 \quad [28]$$

Charge-transfer equations.—Since we neglect any changes in the concentration of CO_3^{2-}, the effect of migration need not be considered. Hence, Ohms' law is valid in both the solid and liquid phases

$$i^{(l)} = -\kappa \nabla \phi^{(l)} \quad [29]$$

$$i^{(s)} = -\sigma \nabla \phi^{(s)} \quad [30]$$

Volume averaging the current in the solid and liquid phases results in the following equations

$$\overline{i^{(l)}} = -\kappa (\varepsilon^{(l)})^{d-1} \nabla (\varepsilon^{(l)} \langle \phi \rangle^{(l)}) \quad [31]$$

$$\overline{i^{(s)}} = -\sigma (\varepsilon^{(s)})^{d-1} \nabla (\varepsilon^{(s)} \langle \phi \rangle^{(s)}) \quad [32]$$

The condition of electroneutrality applies everywhere within the electrode. This means that the net sum of the solution and solid-phase currents should be constant

$$\nabla \cdot (\overline{i^{(l)}} + \overline{i^{(s)}}) = 0 \quad [33]$$

Further, any current leaving the solid phase has to enter the liquid phase through the electrochemical reaction. Applying a balance on the solution-phase current gives

$$\nabla \cdot \overline{i^{(l)}} = a^{(sl)} \langle j_k \rangle^{(sl)} \quad [34]$$

In the above equation the gradient in the solution-phase current is proportional to the reaction rate at the solid-liquid interface. Substituting Eq. 34 into Eq. 33 we have

$$\nabla \cdot \overline{i^{(s)}} = -a^{(sl)} \langle j_k \rangle^{(sl)} \quad [35]$$

Next, we define the overpotential as $\langle \phi \rangle = \langle \phi \rangle^{(s)} - \langle \phi \rangle^{(l)}$. Combining Eq. 31-35 and using the definition for overpotential results in

$$\frac{\partial^2 \langle \phi \rangle}{\partial x^2} = a^{(sl)} \langle j_k \rangle^{(sl)} \left(\frac{1}{\sigma (\varepsilon^{(s)})^d} + \frac{1}{\kappa (\varepsilon^{(l)})^d} \right) \quad [36]$$

Governing equations.—Combining the above set of equation, assuming steady state, and introducing the dimensionless variables we arrive at the following governing model equations

$$\frac{\partial}{\partial x^*} \cdot \left[D_i^{(l)} (\varepsilon^{(l)})^{b-1} \frac{\partial}{\partial x^*} (\varepsilon^{(l)} u_i^{(l)}) \right] - \frac{a^{(lg)} k_i^{(lg)} L^2}{K_{e,i}} (u_i^{(l)} - u_i^{(g)}) - \frac{s_{ik} a^{(sl)} L^2}{n_k F \langle c \rangle_i^{(l)*}} \langle j_k \rangle^{(sl)} = 0 \quad [37]$$

$$D_i^{(g)} \frac{\partial}{\partial x^*} \cdot \left[(\varepsilon^{(g)})^{b-1} \frac{\partial}{\partial x^*} (\varepsilon^{(g)} u_i^{(g)}) \right] - D_i^{(g)} \frac{\partial}{\partial x^*} \left\{ (\varepsilon^{(g)})^{b-1} \frac{u_i^{(g)}}{\langle c \rangle_{CO_2}^{(g)*} u_{CO_2}^{(g)} + \langle c \rangle_{O_2}^{(g)*} u_{O_2}^{(g)}} \frac{\partial}{\partial x^*} \times [\varepsilon^{(g)} (\langle c \rangle_{CO_2}^{(g)*} u_{CO_2}^{(g)} + \langle c \rangle_{O_2}^{(g)*} u_{O_2}^{(g)})] \right\} + L^2 a^{(lg)} k_i^{(lg)} (u_i^{(l)} - u_i^{(g)}) = 0 \quad [38]$$

$$\frac{\partial^2 F \langle \phi \rangle / RT}{\partial x^{*2}} = a^{(sl)} L^2 \langle j_k \rangle^{(sl)} \left(\frac{1}{\sigma (\varepsilon^{(s)})^d} + \frac{1}{\kappa (\varepsilon^{(l)})^d} \right) \frac{F}{RT} \quad [39]$$

The following dimensionless variables have been used in arriving at these equations

$$u_i^{(l)} = \frac{\langle c \rangle_i^{(l)}}{\langle c \rangle_i^{(l)*}}, \quad u_i^{(g)} = \frac{\langle c \rangle_i^{(g)}}{\langle c \rangle_i^{(g)*}}$$

Since we consider the transport of O_2 and CO_2 in the liquid and gas phases, we have five governing equations, four transport equations (Eq. 37 and 38), and one equation for the polarization (Eq. 39). We assume the problem is one-dimensional and neglect any changes in planes perpendicular to the x axis.

Boundary conditions.—Since the gases are fed at the current collector side of the cathode, in the gas phase the concentrations are equal to the inlet concentration. In the solution phase, the concentrations are given by Henry's law. At the electrolyte tile (matrix) side the flux of all species is equal to zero. Also all the current is carried by the ions at the matrix end and by electrons at the current collector end. Based on these conditions the boundary condition at the current collector is given by

$$\langle c_i \rangle^{(l)} = \langle c_i \rangle^{(l)*}, \ \langle c_i \rangle^{(g)} = \langle c_i \rangle^{(g)*}, \ \frac{\partial \langle \phi \rangle}{\partial x} = -\frac{I}{\sigma (\varepsilon^{(s)})^d} \quad \text{at } x = 0 \quad [40]$$

At the matrix ($x = L$)

$$\frac{\partial \langle c_i \rangle^{(l)}}{\partial x} = 0$$

$$(\varepsilon^{(g)})^{b-1} \left[\frac{\partial}{\partial x} (\varepsilon^{(g)} \langle c_i \rangle^{(g)}) + \left\langle \frac{c_i^{(g)}}{c^{(g)}} \right\rangle \frac{\partial}{\partial x} (\varepsilon^{(g)} \langle c \rangle^{(g)}) \right] = 0$$

$$\frac{\partial \langle \phi \rangle}{\partial x} = \frac{I}{\kappa (\varepsilon^{(l)})^d} \quad [41]$$

Expressing them in terms of the dimensionless variables

$$u_i^{(l)} = 1, \ u_i^{(g)} = 1, \ \frac{\partial F \langle \phi \rangle / RT}{\partial x^*} = -\frac{IL}{\sigma (\varepsilon^{(s)})^d} \frac{F}{RT} \quad \text{at } x^* = 0 \quad [42]$$

$$\frac{\partial u_i^{(l)}}{\partial x^*} = 0$$

$$(\varepsilon^{(g)})^{b-1} \left\{ \frac{\partial}{\partial x^*} (\varepsilon^{(g)} u_i^{(g)}) + \left\langle \frac{u_i^{(g)}}{\langle c \rangle_{CO_2}^{(g)*} u_{CO_2}^{(g)} + \langle c \rangle_{O_2}^{(g)*} u_{O_2}^{(g)}} \right\rangle \frac{\partial}{\partial x^*} [\varepsilon^{(g)} (\langle c \rangle_{CO_2}^{(g)*} u_{CO_2}^{(g)} + \langle c \rangle_{O_2}^{(g)*} u_{O_2}^{(g)})] \right\} = 0$$

Table I. List of parameters used in model simulations.

Parameter	Value	Ref.
Diffusion coefficient of CO_2 in the liquid phase, $D^{(l)}_{CO_2}$	$1e^{-3}$ cm^2/s	8
Diffusion coefficient of O_2 in the liquid phase, $D^{(l)}_{O_2}$	$3e^{-3}$ cm^2/s	8
Diffusion coefficient of CO_2 in the gas phase, $D^{(g)}_{CO_2}$	1.16 cm^2/s	17
Diffusion coefficient of O_2 in the gas phase, $D^{(g)}_{O_2}$	1.16 cm^2/s	17
Electrode conductivity, σ	13 S/cm	9
Electrolyte conductivity, κ	$2.0e^{-2}$ S/cm	8
Correction for diffusion coefficient, b	1.5	13
Correction for conductivity, d	1.5	13
Rate constant of the molar flux of CO_2 between the liquid and gas phase, $k^{(lg)}_{CO_2}$	$3e^{-3}$ cm/s	13
Rate constant of the molar flux of O_2 between the liquid and gas phase, $k^{(lg)}_{O_2}$	$2e^{-3}$ cm/s	13
Thickness of the electrode, L	0.06 cm	Measured
Liquid porosity, $\varepsilon^{(l)}$	0.3	Measured
Gas porosity, $\varepsilon^{(g)}$	0.4	Measured
Solid porosity, $\varepsilon^{(s)}$	0.3	Measured
Exchange current density, i^0_0	50 mA/cm^2	20
Cathodic transfer coefficient, α_c	0.5	3, 16
Cathodic transfer coefficient, α_a	1.5	3, 16
r_1	-1.25	3, 16
r_2	0.375	3, 16

$$\frac{\partial F\langle\varphi\rangle/RT}{\partial x} = \frac{IL}{\kappa(\varepsilon^{(l)})^d}\frac{F}{RT} \quad \text{at } x^* = 1 \qquad [43]$$

Based on these equations the following dimensionless groups can be written

$$\delta = a^{(sl)}L^2 i_0\left(\frac{1}{\sigma(\varepsilon^{(s)})^d} + \frac{1}{\kappa(\varepsilon^{(l)})^d}\right)\frac{F}{RT} \qquad [44]$$

$$\gamma_1 = \frac{IL}{\sigma(\varepsilon^{(s)})^d}\frac{F}{RT} \qquad [45]$$

$$\gamma_2 = \frac{IL}{\kappa(\varepsilon^{(l)})^d}\frac{F}{RT} \qquad [46]$$

List of parameters.—The parameters used in the model are given in Table I. Gas-phase diffusion coefficients were estimated using the Fuller correlation.[17] It can also be estimated using the Chapman-Enskong equation. According to the Fuller correlation

$$D = \frac{10^{-3}T^{1.75}(1/M_{CO_2} + 1/M_{O_2})^{1/2}}{p[(V_{CO_2})^{1/3} + (V_{O_2})^{1/3}]^2} \qquad [47]$$

The diffusion volumes have been listed by Cussler[17] as $V_{CO_2} = 26.9$ and $V_{O_2} = 16.6$. At 923 K and 1 atm the binary diffusion coefficient has been estimated as 1.16 cm^2/s.

Experimental

Electrochemical half-cells (3 cm^2) were assembled using two identical $LiNiCoO_2$ cathodes in an alumina housing. The electrodes were prepared by tape-casting followed by sintering at around 900°C. The two electrodes were separated by a $LiAlO_2$ matrix impregnated with a eutectic mixture of 62:38 mol % Li_2CO_3 and K_2CO_3. Gold wire inserted in an alumina tube served as a reference electrode in 33:66 O_2:CO_2 atmosphere. The working temperature of 650°C was reached in a programmed manner in about 50 h. A gas mixture comprising N_2, O_2, and CO_2 was passed at both working and the counter electrodes. The polarization is measured for different applied currents using the current interrupt technique and is corrected to get the IR-free polarization.

Results and Discussion

The model equations are highly nonlinear and coupled in nature and hence cannot be solved analytically. The five governing equations (Eq. 37-39) with the appropriate boundary conditions (Eq. 40 and 41) have been solved simultaneously using Femlab 2.1 (a commercial software package based on finite element analysis) and also using Newman's Band(j). In studying the performance of the cathode, the main parameter of interest is the electrode polarization under different applied currents. The measured polarization is the difference in potential between the current collector $(\Phi_M)_o$ under load as compared to at open circuit $(\Phi_M)_{o,OCV}$. However, the model solves for the local overpotential ϕ, which is the difference between the solid-phase and liquid-phase potential. Lee *et al.*[9] present a relationship between this overpotential and the experimentally measured polarization loss $(\Phi_{Mo}\text{-}\Phi_{Mo,OCV})$. The IR-free polarization is given as

$$\phi_{IR\text{-}free} = (\Phi)_0 + \frac{1}{1 + \kappa_{app}/\sigma_{app}}[(\Phi)_L - (\Phi)_0] \qquad [48]$$

where κ_{app} and κ_{app} are the apparent conductivities modified by the porosity. $(\Phi)_L$ and $(\Phi)_0$ are the overpotentials at the matrix side and the current collector side of the electrode as defined by Lee *et al.*[9] Using the model we studied the effect of different parameters on the IR-free polarization loss.

Effect of conductivity.—Ohmic losses in the MCFC cathode can arise due to poor conductivity of either the electrode or the electrolyte. The electrolyte here is an eutectic mixture of Li_2CO_3-K_2CO_3 held in a lithium aluminate matrix. The electrolyte fills inside the porous cathode due to capillary forces. In general the conductivity of the electrode material is much larger than that of the electrolyte. The conductivity of the melt lies in the order of 10^{-2} S/cm while solid-phase (electrode) conductivities are in the order of 10 S/cm. Figure 3 presents the polarization loss at various loads for different values of the electrolyte conductivity. The model simulations were run with a σ value of 13 S/cm. From Fig. 3 it can be seen that increase in κ decreases the polarization loss. At large values of κ (2.0 S/cm) a linear relationship is seen between the polarization loss and the applied load. With decreasing values of κ, the polarization loss increases exponentially with increasing applied current. For

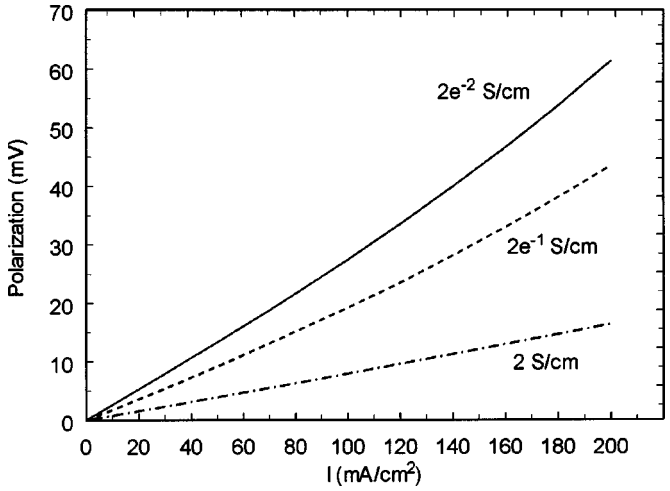

Figure 3. Effect of electrolyte conductivity on the polarization behavior of MCFC cathode. Parameters used in the simulation are given in Table I.

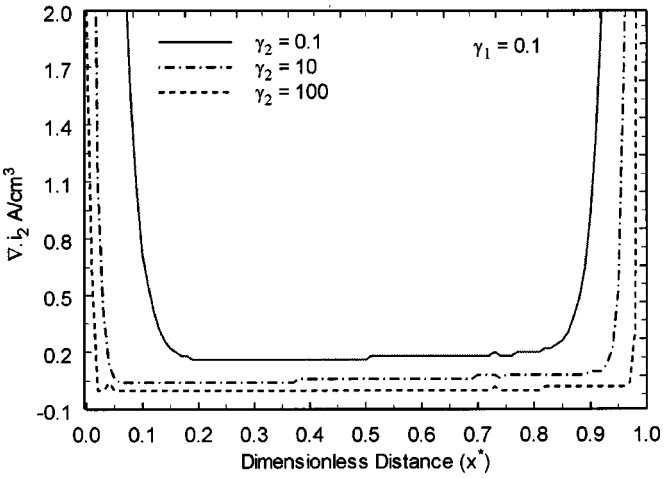

Figure 5. Changes in the electrode reaction rate for varying electrolyte conductivity. The parameters γ_1 and γ_2 are given by Eq. 45 and 46.

$\kappa = 2.0 \times 10^{-2}$ S/cm it can be seen that changing the applied current from 160 mA/cm^2 to 200 mA/cm^2 results in increasing the polarization loss by 15 mV. A similar change in current for $\kappa = 2.0$ S/cm would increase the polarization loss only by 3 mV. While the model simulations show a significant effect of the electrolyte conductivity on electrode performance, in reality the choice of electrolyte is limited by other considerations. Stability at high temperatures, low dissolution of cathode material, and current collector in the melt play a critical role in limiting the choice to a few eutectic mixtures. While the difference in conductivity between these different melts is not significant, the effective electrolyte conductivity depends strongly on the cathode design. The effective electrolyte conductivity is affected by the degree of electrolyte fill in the cathode, which in turn is influenced by the number of macropores and micropores in the cathode. In order to study this we plot the local overpotential across the thickness of the electrode for different κ values. As seen from Fig. 4, the difference between the solid- and liquid-phase potentials increases with the increase in distance from the current collector. With decreasing values of κ most of the polarization drop occurs close to the matrix.

Figure 5 and 6 present the change in reaction rate di_2/dx across the thickness of the electrode. The variable di_2/dx is a measure of the reaction rate or the current transferred per unit volume ($a^{(sl)}\langle j_k\rangle^{(sl)}$) and is given by Eq. 34. The reaction rate is plotted as a function of two different dimensionless parameters, γ_1 and γ_2, as defined by Eq. 45 and 46. The parameters γ_1 and γ_2 are a measure of the electrode and electrolyte resistivity, respectively. As seen from Fig. 5 changes in γ_2 have a significant effect on the reaction rate di_2/dx. These simulations have been done after fixing the ohmic conductivity of the electrode, *i.e.*, γ_1. With increase in γ_2 (high electrolyte resistance), the reaction rate remains close to zero in most parts of the electrode. In general it is preferable to have an electrode with a uniform reaction rate distribution everywhere. The model simulations indicate that if γ_1 and γ_2 differ significantly (over two orders of magnitude) most of the reaction occurs within a zone close to the current collector and electrolyte matrix. The rest of the electrode does not take part in the reaction, and this represents a loss of effective active material. Figure 6 presents the model results when the electrolyte conductivity (γ_2) is fixed and the electrode conductivity (γ_1) is varied. In both Fig. 5 and Fig. 6, it can be seen that when γ_1 and γ_2 are comparable to each other the reaction rate does not go to zero across the electrode. However, both low electrode and electrolytic conductivity lead to very poor reaction rate distribution across the electrode. For all cases, the reaction rate remains high close to the current collector and matrix. When the elec-

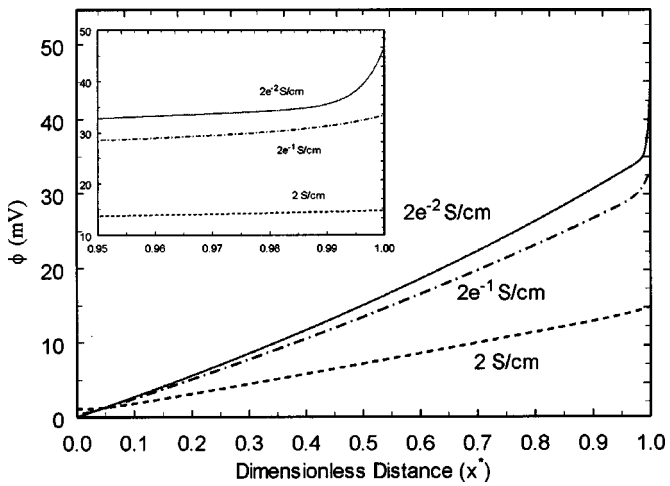

Figure 4. Comparison of overpotential profiles for different κ values. The overpotential is defined as $\langle\phi\rangle = \langle\phi\rangle^{(s)} - \langle\phi\rangle^{(l)}$. Inset shows the profiles closer to the electrolyte tile.

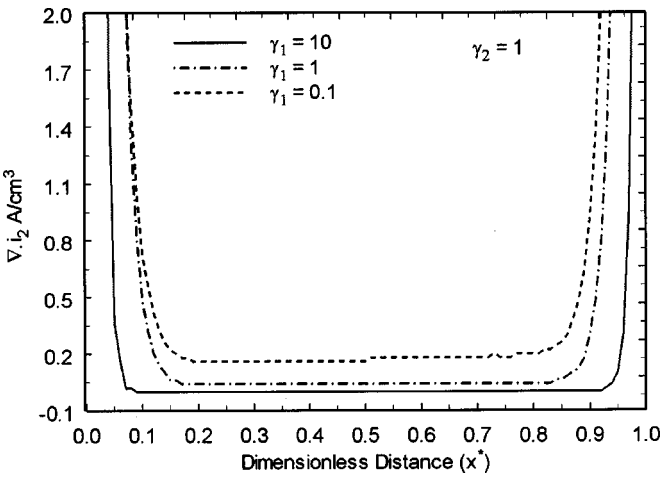

Figure 6. Comparison of reaction rates for varying electrode conductivities.

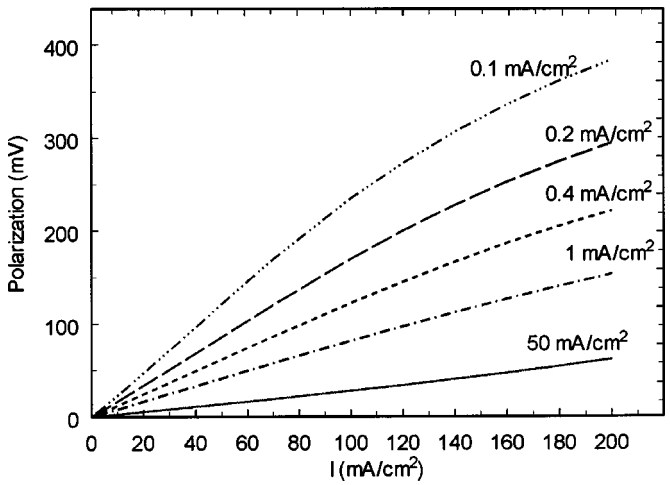

Figure 7. Effect of exchange current densities on the polarization behavior of the MCFC cathode.

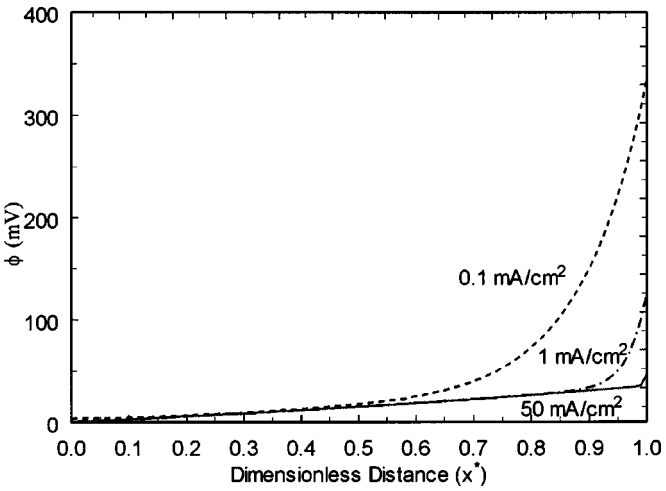

Figure 8. Change in local overpotential along the length of the electrode. Profiles are shown for different values of the exchange current density.

trolytic and ohmic conductivities are equal to each other a symmetrical reaction rate distribution curve is obtained. This is similar to the analysis given by Newman and Tobias[18] for porous electrodes. Although a uniform reaction distribution is the desirable scenario practical considerations limit us from achieving this. As mentioned before, in general solid-phase conductivities are much larger than liquid-phase conductivities. Hence, the actual electrode utilization is not 100% but much lower than that. Using this theoretical model it is possible to optimize the electrode thickness based on input electrode parameters.

Effect of exchange current density.—We next study the effect of reaction kinetics on the electrode performance. Various mechanisms have been proposed for the cathode reaction in MCFC. While the exact nature of the reaction is under discussion, the rate of the reaction can be measured easily. Similar to electrode conductivity, the oxygen reduction rate varies significantly on different materials. The state-of-the-art cathode material in MCFC is NiO with a reported i_0^0 value of $0.81\ \mathrm{mA/cm^2}$.[9] Alternate materials such as $LiCoO_2$ ($i_0^0 = 0.5\ \mathrm{mA/cm^2}$)[9] and $LiFeO_2$ ($i_0^0 = 0.1\ \mathrm{mA/cm^2}$)[9] have been tested as cathodes since they exhibit lower corrosion rates in the melt. Figure 7 presents the polarization loss at different currents for various i_0^0 values. As seen from the plot, varying i_0 has a significant effect on the polarization loss. As i_0^0 decreases the overpotential increases as a result of increased kinetic resistance as shown in Fig. 8. Similar to κ at high values of i_0^0, the polarization loss increases linearly with increasing applied loads. However, at low values of i_0^0 the polarization loss increases asymptotically and reaches a plateau with an increase in current. This is in contrast to Fig. 4 where decrease in kappa increases the potential drop exponentially. As i_0 decreases, the reaction rate also decreases. Due to the slower reaction rate, mass transfer becomes competitive with reaction kinetics. Hence increasing the current density does not translate into increased polarization loss. These results agree well with those reported earlier by Lee *et al.*[9] Figure 8 shows the overpotential profiles for different exchange current densities. The simulations were performed for an applied current of $160\ \mathrm{mA/cm^2}$. The overpotential increases sharply near the matrix side of the electrode. It can also be seen that the large potential drop close to the electrolyte matrix increases with decrease in i_0^0. This directly translates to a large polarization drop across the electrode (see Fig. 7). In our simulations we assumed that a di_2/dx value less than 5% of the maximum reaction rate indicated a dead zone with no reaction. The percent utilization of the active material is calculated for different i_0^0 using this baseline (5% of the maximum reaction rate). Figure 9 shows the percent utilization of the electrode material as a function of the exchange current density. It can be clearly seen that as i_0 increases the utilization decreases indicating that only a small fraction of the electrode takes part in the reaction. Most of the reaction takes place in a small part of the electrode near the electrolyte tile. Figure 6 shows that materials with high i_0^0 values have low polarization drops. However, from Fig. 9 it can be seen that an increase in i_0^0 translates to poor utilization of active material. For small i_0^0 values, the reaction rate is slow and hence this allows sufficient time for dissolved O_2 and CO_2 to reach the active solid interface and react. The slow reaction rate also allows the reaction to take place much deeper within the electrode as compared to at high reaction rate. Both these factors contribute to the higher utilization observed for low i_0^0 values.

Effect of diffusion coefficient.—The reactants in the gas phase diffuse from the gaseous macropore to the catalyst surface through the micropore, which has the electrolyte. Here we study the effect of mass transfer through the electrolytic phase. Figure 10 presents a comparison of the liquid-phase carbon dioxide concentration across the electrode for different values of the diffusion coefficient. It can be seen that change in the liquid-phase diffusion coefficient signifi-

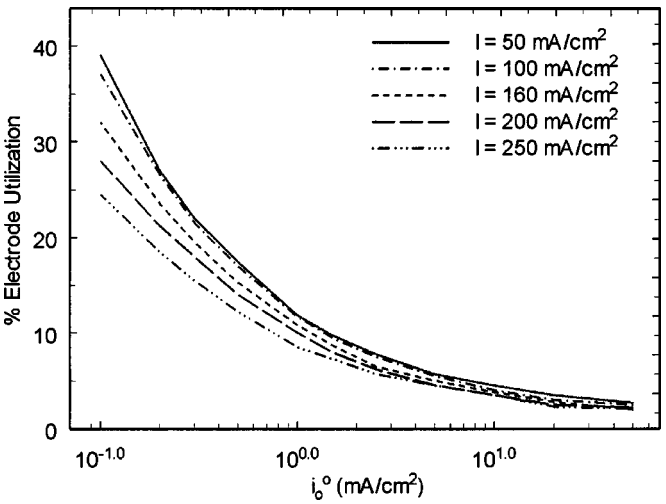

Figure 9. Change in the electrode utilization as a function of exchange current density. Profiles are shown for different applied currents.

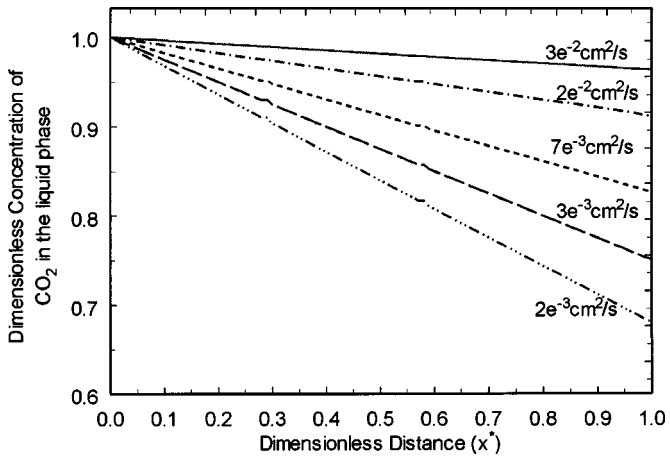

Figure 10. Steady-state CO_2 liquid-phase concentration profiles across the length of the MCFC cathode for different values of the liquid-phase diffusion coefficient.

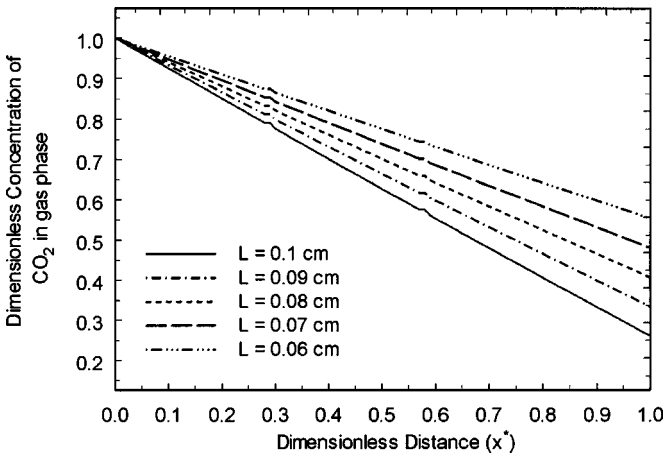

Figure 12. Change in the gas-phase CO_2 concentration for varying electrode thickness.

cantly alters the concentration across the electrode. At very low values (10^{-4} cm^2/s) of $D_i^{(l)}$ the O_2 and CO_2 concentration close to the matrix drops to zero (not shown in figure). However, the diffusion coefficient for both dissolved oxygen and carbon dioxide in MCFC cathodes lies in the order of 10^{-3} to 10^{-2} cm^2/s.[8] From Fig.10 it can be seen that at this value of the diffusion coefficient no depletion of dissolved CO_2 occurs anywhere within the electrode. A linear concentration gradient exists across the thickness of the electrode for both O_2 and CO_2. The overpotential is almost uniform for large diffusion coefficients whereas for small diffusion coefficients the overpotential increases drastically very near the matrix region (not shown in figure). A similar effect is seen by varying both O_2 and CO_2 diffusion coefficients. Also, simulation results show that changing the diffusion coefficient by one order of magnitude results in an increase in polarization of only 20 mV. This effect is smaller than that seen for electrolyte conductivity and exchange current density. These results indicate that mass transfer in the liquid phase is not rate-limiting for MCFC cathodes.

Effect of thickness of the electrode.—The resistance to mass transfer increases as the electrode thickness increases. Hence the polarization increases with the thickness as shown in Fig. 11. This agrees with the prediction by Prins-Jansen *et al.*[3] Their simulations considered changing the thickness keeping all other parameters constant similar to what has been done here. As suggested by Prins-Jansen *et al.*[3] increasing the thickness has two conflicting effects, both the mass-transfer resistance and the active surface area are being increased. The upward bending effect seen in Fig. 11 is due to the increase in the mass-transfer resistance. Due to the competing effects of mass transfer and increase in surface area, the polarization loss should go through an optimum as the electrode thickness is increased. However, both in our model simulations and in Prins-Jansen *et al.*[3] we observe a monotonic dependency where polarization loss always increases with increase in thickness. This can be attributed to the assumption involved in the model simulation, *i.e.*, the active surface area does not change with an increase in thickness.

Fontes *et al.*[11] state that optimum electrode thickness is shifted towards thicker electrodes as the electrolyte conductivity increases. Increase in κ increases the utilization of the active material as shown in Fig. 4. Hence the thickness of the electrode can be increased with increased electrolyte conductivity to obtain similar performance. Figure 12 plots the CO_2 gas-phase concentration across the electrode thickness. It can be seen that even under high utilization (40-60%) all the gas in the electrode is not consumed. For an electrode

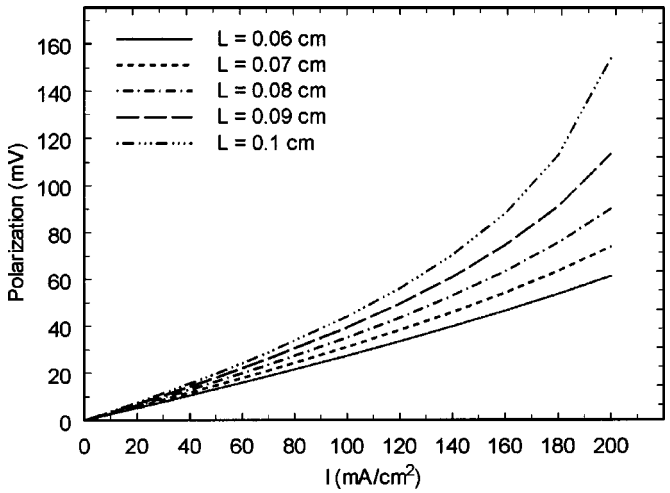

Figure 11. Effect of electrode thickness on the polarization loss at different applied loads.

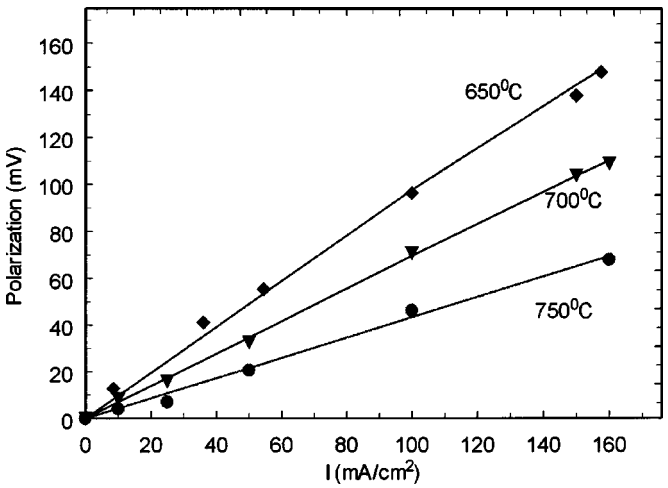

Figure 13. Change in $LiNiCoO_2$ electrode polarization with applied current density for different temperatures. Solid lines are model simulations and symbols represent experimental data. Thermodynamic, kinetic, and transport parameters extracted from the fitting are presented in Table II.

Table II. Temperature dependence of different electrode parameters for $LiNiCoO_2$ cathode.

Parameter	a	b (1/K)	R^2
κ	3.268 S/cm	4715.5	0.9915
$D^l_{CO_2}$	144.82 cm^2/s	10975	0.9994
$D^l_{O_2}$	0.352 cm^2/s	4417	0.9751
i^0_0	243.96 A/cm^2	11887	0.9842

thickness of 0.6 mm close to 40% of the inlet gas is still available at the outlet. In MCFC stacks, it has been estimated that the utilization of the oxidant gases is around 40-50%. The change in gas-phase concentration does not have a significant effect on the electrode performance at high gas flow rates. However, decrease in both oxygen and carbon dioxide flow rate will affect the performance of the cathode. The liquid phase reactant concentrations are directly dependent on the gas concentration in the macropore at that point. Low flow rates contribute to high utilization thereby leading to a decrease in gas-phase concentration. This will decrease the amount of reactant available for taking part in the reduction reaction at the solid/liquid interface and hence increase the polarization loss as seen in Fig. 11.

Comparison of model to experimental data.—Figure 13 compares the model to our experimental data of $LiNiCoO_2$ at different temperatures. With an increase in temperature the reaction rate as given by the exchange current density and the species transport rate as given by the diffusion coefficient increase. Further the electrolyte conductivity also increases. The gas-phase diffusion coefficients at different temperatures can be calculated using the Fuller correlation.[17] The temperature dependency of the liquid-phase diffusion coefficients, electrolyte conductivity, and the exchange current density were determined by fitting the model to the experimental data. In all cases an Arrhenius relationship to the temperature was obtained. The fitting results along with the R^2 term are given in Table II. The dependence is given by

$$x = a \exp\left(-\frac{b}{T}\right)$$

The parameters obtained from fitting the model data were used in the subsequent simulations. Our next goal was to compare the polarization behavior of the cathode under different gas compositions.

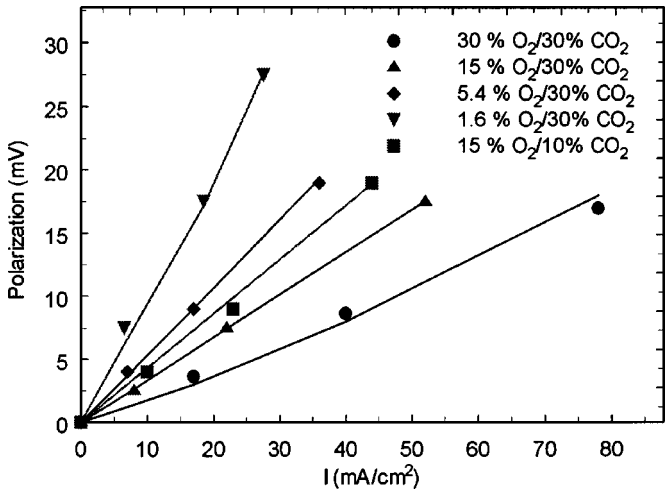

Figure 14. Comparison of model results and experimental data for different gas compositions. Experimental data were obtained from the polarization behavior for $LiCoO_2$ given by Lagergren and Simonsson.[19]

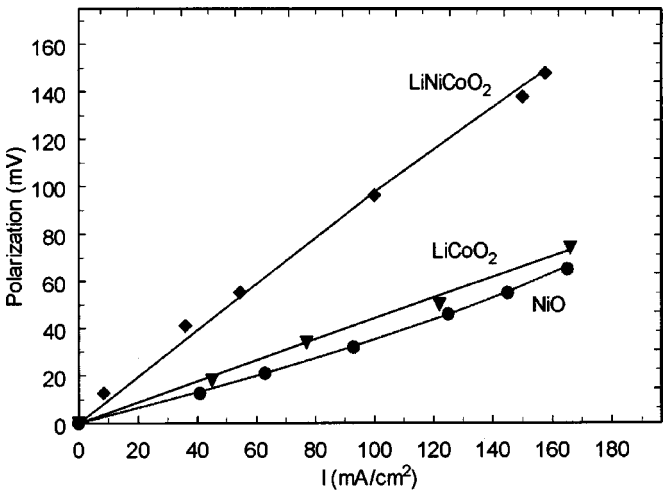

Figure 15. Comparison of model to experimental polarization data for different cathode materials.

Our model predicts monotonic dependence of the polarization loss on both CO_2 and O_2 partial pressure. The exchange current density is concentration dependent and has a negative reaction order dependence for CO_2 and positive order dependence for O_2. Increasing the concentration of CO_2 decreases the local current density and hence increases the polarization. The effect is the reverse for O_2. Similar results have been obtained by previous researchers also. This is shown in Fig. 14, which gives the fit of our model to experimental data of $LiCoO_2$ at low overpotentials obtained by Lagergren and Simonsson[19] for different gas compositions. The model parameters remained the same as for $LiNiCoO_2$ (see Table II) except for the exchange current density, which was calculated as 5 mA/cm^2 at 650°C.

Figure 15 presents comparison of polarization profiles between three different cathode materials, namely, NiO, $LiCoO_2$, and $LiNiCoO_2$. For all three cathode materials good agreement is seen between model simulations and experimental data. NiO is a p-type semiconductor and has a lower conductivity than pure Ni. Li^+ ions coming from the electrolyte, diffuse into the NiO and increase its electronic conductivity. However, NiO has a much larger exchange current density for oxygen reduction as compared to alternate cathode materials such as $LiNiCoO_2$ and CoO_2. Model simulations indicate that an electrode made of a material, which has the conductivity of NiO, and exchange current density of $LiCoO_2$ would suffer around 100% more polarization than the conventional NiO cathode. The exchange current density and electrode conductivity of the three materials obtained using the homogeneous model are given in Table III. These results show that the model can be used to extract critical thermodynamic, kinetic, and transport parameters from polarization data.

Conclusions

The electrolyte conductivity and exchange current density have very large effects on the performance of the MCFC cathode as compared to other parameters. Due to low electrolyte conductivity as

Table III. Kinetic and conductivity properties for different cathode materials.

Cathode material	σ (S/cm)	i_o (mA/cm^2)
NiO	13	50
$LiCoO_2$	1	5
$LiNiCoO_2$	5	0.65

compared to solid-phase conductivity, most of the polarization loss occurs in a region close to the electrolyte matrix. Most of the material within the center of the electrode does not take part in the electrochemical reaction. This leads to low active material utilization within the electrode. Both low electrode and electrolytic conductivity lead to very poor reaction rate distribution across the electrode.

An increase in reaction rate as exemplified by the exchange current density leads to a decrease in polarization losses. Further, with increase in i_0^0 the polarization loss increases linearly with increasing applied loads. However, at low values of i_0^0 the polarization loss increases asymptotically and reaches a plateau with increase in current.

The amount of active material utilized also varies with exchange current density. At high values of i_0^0 (>10 mA/cm^2), irrespective of the applied load most of the reaction takes place in a small part of the electrode near the electrolyte matrix and hence only 5% of the electrode is utilized. For small i_0^0 values the reaction rate is slow and hence this allows sufficient time for dissolved O_2 and CO_2 to reach the active solid interface and react. The slow reaction rate also allows the reaction to take place much deeper within the electrode as compared to at high reaction rates. Both these factors contribute to the higher utilization observed for low i_o values.

Changes in both gas-phase and liquid-phase diffusion coefficient do not have a significant effect on the polarization characteristics. In general, in the polarization curve a downward bending effect is observed due to kinetic limitations and an upward bending effect due to mass-transfer limitations. Under normal operating conditions mass transfer is not rate limiting and the electrode is generally under mixed control.

The diffusion coefficients, electrolyte conductivity, and the exchange current density are all affected by changes in temperature. All of them have an Arrhenius form of dependency on temperature. The activation energy and the frequency factor for each of these parameters have been estimated by fitting the model to experimental data of $LiNiCoO_2$ at different temperatures. Using these fitted parameters the performance of NiO and $LiCoO_2$ cathodes has been studied. The exchange current density for different materials was obtained by fitting the model to the experimental polarization data. Hence, apart from qualitative analysis of the cathode behavior, the model can be used to extract critical thermodynamic, kinetic, and transport parameters from polarization data.

A key parameter whose effect on the behavior of the electrode has not been considered is electrolyte filling. Increasing the amount of electrolyte within the MCFC cathode increases the conductivity, but reduces the mass-transfer rate. Simulations were run by increasing $\varepsilon^{(l)}$ and decreasing $\varepsilon^{(g)}$ to account for the increase in electrolyte fill. Results from our model show that the polarization drops with increasing electrolyte filling. There was no optimum as seen experimentally. The model simulations were obtained by keeping all parameters except the porosities constant. Any modifications to the electrolyte content will change the interfacial surface areas ($a^{(sl)}$ and $a^{(gl)}$), which has not been accounted for in these simulations. Mercury porosimetry yields information on the active surface areas corresponding to micropores and macropores and also the liquid and gas porosity. Assuming that the micropores are flooded with electrolyte and macropores with gas, we can determine values for $a^{(sl)}$ and $a^{(gl)}$.

These two parameters along with the porosities can be input into the model to determine the polarization behavior. In future, we plan to extend the homogeneous model to account for electrolyte filling by using data from mercury porosimetry.

Acknowledgments

Financial support by the National Energy Technology Laboratory, which is supported by the U.S. Department of Energy, is gratefully acknowledged.

University of South Carolina assisted in meeting the publication costs of this article.

List of Symbols

$\langle CO_2\rangle^g$	volume averaged concentration of CO_2 in the gas phase, mol/cm^3
$\langle O_2\rangle^g$	volume averaged concentration of O_2 in the gas phase, mol/cm^3
$\langle CO_2\rangle^l$	volume averaged concentration of CO_2 in the liquid phase, mol/cm^3
$\langle O_2\rangle^l$	volume averaged concentration of O_2 in the liquid phase, mol/cm^3
$\langle CO_2\rangle^{(g)*}$	bulk concentration of CO_2 in the gas phase, mol/cm^3
$\langle O_2\rangle^{(g)*}$	bulk concentration of O_2 in the gas phase, mol/cm^3
$\langle CO_2\rangle^{(l)*}$	bulk concentration of CO_2 in the liquid phase, mol/cm^3
$\langle O_2\rangle^{(l)*}$	bulk concentration of O_2 in the liquid phase, mol/cm^3
$a^{(lg)}$	specific surface area at the gas/liquid interface, cm^2/cm^3
$a^{(sl)}$	specific surface area at the liquid/solid interface, cm^2/cm^3
b	correction for diffusion coefficeint
c	total concentration, mol/cm^3
$c_i^{(k)}$	concentration of species i in phase k, mol/cm^3
d	correction for conductivity
$D_{(AB)}$	diffusion coefficient of A into B, cm^2/s
$D_{CO_2}^{(g)}$	diffusion coefficient of CO_2 in the gas phase, cm^2/s
$D_{O_2}^{(g)}$	diffusion coefficient of O_2 in the gas phase, cm^2/s
$D_{CO_2}^{(l)}$	diffusion coefficient of CO_2 in the liquid phase, cm^2/s
$D_{O_2}^{(l)}$	diffusion coefficient of O_2 in the liquid phase, cm^2/s
$\overline{F}_i^{(lg)}$	average flux of species i from the liquid phase into the gas phase, mol/cm^3 s
I	applied current, A/cm^2
i_0^0	concentration independent exchange current density, A/cm^2
i_0	concentration dependent exchange current density, A/cm^2
$i^{(l)}$	current density in the electrolyte, A/cm^2
$i^{(s)}$	current density in the solid, A/cm^2
$\overline{i}^{(l)}$ (or i_2)	volume averaged current density in the electrolyte, A/cm^2
$\overline{i}^{(s)}$	volume averaged current density in the solid, A/cm^2
$J_{(i)}^{\diamond}$	molar flux of species i relative to molar average velocity, mol/cm^2 s
$j_{(i)}^{\diamond}$	mass flux of species i relative to molar average velocity, mol/cm^2 s
$j_{(i)}$	mass flux of species i relative to mass average velocity, mol/cm^2 s
$\langle j_k\rangle^{(sl)}$	average local current density due to reaction k taking place at the liquid/solid interface, A/cm^2
K_{e,CO_2}	equilibrium constant relating the concentration of CO_2 in the liquid and gas phase, $\langle c^*_{CO_2}\rangle^{(l)}/\langle c^*_{CO_2}\rangle^{(g)}$
K_{e,O_2}	equilibrium constant relating the concentration of O_2 in the liquid and gas phase, $\langle c^*_{O_2}\rangle^{(l)}/\langle c^*_{O_2}\rangle^{(g)}$
$k_{CO_2}^{(lg)}$	rate constant of molar flux of CO_2 between the liquid and gas phase, cm/s
$k_{O_2}^{(lg)}$	rate constant of molar flux of O_2 between the liquid and gas phase, cm/s
L	thickness of the electrode, cm
$M_{(i)}$	molecular weight of species i, g/mol
N_i	molar flux of species i with respect to a fixed frame of reference, mol/cm^2 s
$N_i^{(k)}$	molar flux of species i in phase k, mol/cm^2 s
$\overline{N}_i^g$	volume averaged molar flux of species i in the gas phase, mol/cm^2 s
$\overline{N}_i^l$	volume averaged molar flux of species i in the liquid phase, mol/cm^2 s
n_k	number of electrons exchanged through reaction k
$\mathbf{n}_{(lg)}$	unit normal vector to the surface $S_{(lg)}$ pointing out of the liquid into the gas phase
$\mathbf{n}_{(ls)}$	unit normal vector to the surface $S_{(ls)}$ pointing out of the liquid into the gas phase
$p^*_{CO_2}$	equilibrium partial pressure of CO_2, atm
$p^*_{O_2}$	equilibrium partial pressure of O_2, atm
p	total pressure, atm
$\overline{R}_i^{ls}$	average rate of production f species i at the liquid/solid interface, mol/cm^3 s
$\overline{R}_i^{(gs)}$	average rate of production f species i at the gas/solid interface, mol/cm^3 s
$r_i^{(lg)}$	molar flux of species i from the liquid into the gas phase, mol/cm^2 s
s_{ik}	stoichiometry of species i in reaction k
$S_{(lg)}$	surface that coincides with the liquid/gas interface inside volume V, cm^2
$S_{(ls)}$	surface that coincides with the liquid/solid interface inside volume V, cm^2
T	temperature, K
$u_i^{(k)}$	dimensionless concentration of species i in phase k
V	volume of porous media, cm^3
$V_{(i)}$	volume of phase i in the porous media, cm^3
V_{CO_2}	diffusion volume of CO_2
V_{O_2}	diffusion volume of O_2
$x_{(i)}$	mole fraction of species i

Greek

α_c cathodic transfer coefficient
α_a anodic transfer coefficient
$\varepsilon^{(g)}$ gas porosity
$\varepsilon^{(l)}$ liquid porosity
$\varepsilon^{(s)}$ solid porosity
κ electrolyte conductivity, S/cm
κ_{app} apparent electrolyte conductivity, S/cm = $\kappa(\varepsilon^{(l)})^d$
σ_{app} apparent electrode conductivity, S/cm = $\sigma(\varepsilon^{(s)})^d$
$\rho_{(i)}$ density of species i, g/cm^3
σ electrode conductivity, S/cm
ν mass average velocity, cm/s
$\nu^{\diamond}$ molar average velocity, cm/s
$\langle\phi\rangle$ overpotential, V
$\phi^{(k)}$ potential in phase *k*, V
$\langle\phi\rangle^{(l)}$ volume averaged liquid-phase potential, V
$\langle\phi\rangle^{(s)}$ volume averaged solid-phase potential, V

Superscripts

l liquid phase
g gas phase

References

1. G. Wilemski, *J. Electrochem. Soc.*, **130**, 117 (1983).
2. C. Y. Yuh and J. R. Selman, *J. Electrochem. Soc.*, **131**, 2062 (1984)
3. J. A. Prins-Jansen, K. Hemmes, and J. H. W de Wit, *Electrochim. Acta*, **40**, 3585 (1997).
4. H. R. Kunz and L. A. Murphy, *J. Electrochem. Soc.*, **135**, 1124 (1988).
5. E. Fontes, C. Lagergren, and D. Simonsson, *Electrochim. Acta*, **38**, 2669 (1993).
6. P. S. Christensen, and H. Livbjerg, *Chem. Eng. Sci.*, **47**, 2933 (1992).
7. E. Fontes, M. Fontes, and D. Simonsson, *Electrochim. Acta*, **141**, 1 (1996).
8. J. A. Prins-Jansen, J. D. Fehribach, K. Hemmes, and J. H. W. de Wit, *J. Electrochem. Soc.*, **143**, 1617 (1996).
9. G. L. Lee, J. R. Selman, and L. Pomp, *J. Electrochem. Soc.*, **140**, 390 (1993).
10. E. Fontes, C. Lagergren, and D. Simonsson, *J. Electroanal. Chem.*, **432**, 121 (1997).
11. E. Fontes, M. Fontes, G. Lindbergh, and D. Simonsson, *J. Appl. Electrochem.*, **27**, 1149 (1997).
12. P. de Vidts and R. E. White, *J. Electrochem. Soc.*, **144**, 1343 (1997).
13. P. de Vidts, Ph.D. Thesis, Texas A & M University, College Park, TX (1995).
14. J. C. Slattery, *Advanced Transport Phenomena*, Cambridge University Press, New York (1999).
15. M. Kaviany, *Principles of Heat Transfer in Porous Media*, Springer-Verlag, New York (1991).
16. J. Prins-Jansen, Ph.D. Thesis, Delft University of Technology, Delft, The Netherlands (1996).
17. E. L. Cussler, *Diffusion, Mass Transfer in Fluid Systems*, Cambridge University Press, New York (1984).
18. J. S. Newman and C. W. Tobias, *J. Electrochem. Soc.*, **109**, 1183 (1962).
19. C. Lagergren and D. Simonsson, *J. Electrochem. Soc.*, **144**, 3813 (1997).
20. C. Y. Yuh, Ph.D. Thesis, Illinois Institute of Technology, Chicago, IL (1985).